Available online at www.sciencedirect.com
ScienceDirect
International Journal of Impact Engineering 35 (2008) 290–303
INTERNATIONAL JOURNAL OF IMPACT ENGINEERING
www.elsevier.com/locate/ijimpeng

Numerical predictions of ballistic limits for concrete slabs using a modified version of the HJC concrete model

M. Polanco-Loria[a,*], O.S. Hopperstad[b], T. Børvik[b,c], T. Berstad[a]

[a]SINTEF Materials and Chemistry, N-7465 Trondheim, Norway
[b]Structural Impact Laboratory (SIMLab), Department of Structural Engineering, Norwegian University of Science and Technology (NTNU), N-7491 Trondheim, Norway
[c]Research & Development Department, The Norwegian Defence Estates Agency, N-0103 Oslo, Norway

Received 12 October 2006; accepted 1 March 2007
Available online 18 March 2007

Abstract

Some modifications to the Holmquist–Johnson–Cook (HJC) model (1993) for concrete under impact loading conditions are proposed. First, the pressure-shear behaviour is enhanced by including the influence of the third deviatoric stress invariant to take into account the substantial shear strength difference between the tensile and compressive meridians. Second, the modelling of strain-rate sensitivity is slightly changed so that the strain-rate enhancement factor goes to unity for zero strain rate. Third, three damage variables describing the tensile cracking, shear cracking and pore compaction mechanisms are introduced. A critical review of the constitutive model with alternative proposals for parameter identification is given. The model parameters are obtained for two concrete qualities, and perforation of concrete slabs is considered numerically and compared with experimental results from the literature. Ballistic limit assessments with deviations under 8% when compared to the experimental results are obtained, indicating that the modified version of the HJC concrete model represents a good compromise between simplicity and accuracy for large-scale computations of concrete plates impacted by projectiles.

Keywords: Concrete plates; Projectile perforation; Elastic-viscoplastic model; Isotropic damage; Numerical simulations

1. Introduction

Concrete is a material frequently used in protective structures. This makes concrete of particular interest for the nuclear industry and fortification installations for defence purposes [1,2]. Many important studies of the behaviour of concrete targets impacted by projectiles have been of an empirical nature and most of the experimental studies have focused on the determination of empirical formulae or simplified analytical models [3–5]. On the other hand, the parallel development of numerical tools (e.g. finite element packages [6–8]) and new constitutive models for concrete has contributed to an increased use of numerical simulations for prediction of penetration and impact problems [9–11]. Different constitutive models for concrete are available for the analysis and design of concrete structures, as described in Refs. [12–14], among others. However, still the development of reliable and robust material laws for concrete subjected to high-intensity loading of short duration is a subject of current research.

Analysis of steel reinforced concrete structures impacted by free-flying projectiles is extremely difficult because of the complex states of stress acting inside the material. Under a multi-axial state of stress the damage mechanisms activated are highly dependent on the loading path imposed. For concrete materials under static loading conditions, Mazars [15] showed that depending on the load path different damage mechanisms are activated; namely cracking, shearing (e.g. mode II cracking) and compaction, as shown in Table 1. In particular, for impact and penetration problems these three mechanisms are always present, as indicated by Bourlion [16] and illustrated in Fig. 1. This requires the development of material models capable

*Corresponding author. Tel.: +47 93 28 04 35; fax: +47 73 59 29 31.
E-mail address: mario.polanco@sintef.no (M. Polanco-Loria).

0734-743X/$ - see front matter © 2007 Elsevier Ltd. All rights reserved.
doi:10.1016/j.ijimpeng.2007.03.001

Table 1
Main damage mechanisms according to Mazars [15]

Damage mechanism	Classical loading
Type of loading A Tension and/or compression with low lateral pressure (uniaxial, biaxial or tri-axial) *Characteristics* Possibility of extension, at least in one principal direction Brittle/softening behaviour *Local damage mode* Cracking mainly in mode I (debonding) and mode I + II (debonding + branching)	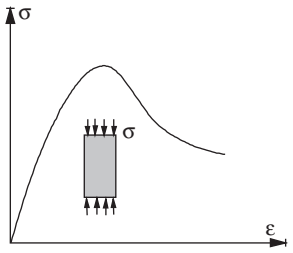
Type of loading B Compression with moderate to high lateral pressure (tri-axial) *Characteristics* No extension "Ductile" behaviour *Local damage mode* Cracking mainly in mode II and III (branching)	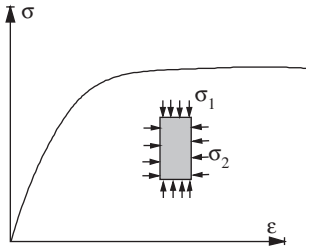
Type of loading C Hydrostatic pressure (tri-axial) *Characteristics* No extension Hardening and stiffening *Local damage mode* Consolidation of the micro-porous structure	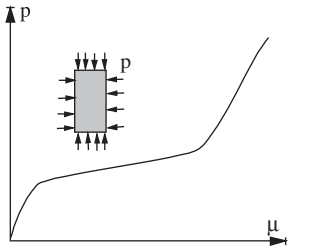

to describe concrete behaviour under low and high confining pressures and the observed differences in rate sensitivity of these mechanisms.

In [12] a literature review of existing experimental data and constitutive models for concrete materials under impact loading conditions was undertaken. It was concluded that the Holmquist, Johnson and Cook (HJC) concrete model [17,18] represents a good compromise between simplicity and accuracy for large-scale computations, and the HJC model was implemented in LS-DYNA [7] for penetration simulations. Some improvements of the original HJC model were recommended and evaluated in [19], which forms the basis of the modified version of the HJC model presented in this work. In particular, the modifications include a continuous function describing the pressure-shear response, the influence of the third deviatoric stress invariant to take into account the difference between the shear response of the tensile and compressive meridians, a non-linear two-parameter equation to handle the strain-rate sensitivity and the introduction of three damage variables describing tensile cracking, shear cracking and pore compaction mechanisms. Because of these modifications of the original model, the present version will be referred to as the MHJC model.

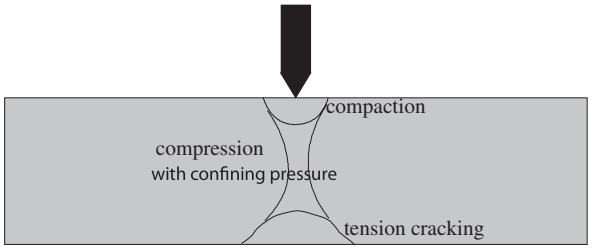

Fig. 1. Schematic description of the mechanisms activated during impact [16].

This paper describes the modifications proposed to the HJC model in some detail. The MHJC model has been implemented into LS-DYNA as a user-material model and is validated against some experimental results for the ballistic perforation resistance of concrete slabs presented in the literature.

2. Original HJC concrete model

The HJC model was originally presented by HJC [17] with the purpose of developing a concrete model for impact computations where the material experiences large strains, high strain rates and high pressures. The HJC concrete model is an elastic-viscoplastic model coupled with isotropic damage, where the response is separated into hydrostatic and deviatoric contributions.

The Cauchy stress tensor σ_{ij} is decomposed into deviatoric and hydrostatic parts

$$\sigma_{ij} = S_{ij} - P\delta_{ij}, \tag{1}$$

where S_{ij} is the stress deviator, $P = -\sigma_{kk}/3$ is the hydrostatic pressure and δ_{ij} is the Kronecker delta. The von Mises equivalent stress is then defined by

$$\sigma_{\text{eq}} = \sqrt{\tfrac{3}{2}S_{ij}S_{ij}}. \tag{2}$$

The deviatoric part D'_{ij} of the rate-of-deformation tensor D_{ij} is defined as

$$D'_{ij} = D_{ij} - \tfrac{1}{3}D_{kk}\delta_{ij} \tag{3}$$

and it is decomposed into its elastic and plastic parts according to

$$D'_{ij} = D'^{\,\text{e}}_{ij} + D'^{\,\text{p}}_{ij}, \quad D'^{\,\text{e}}_{ij} = \frac{1}{2G}S^{\nabla J}_{ij}, \quad D'^{\,\text{p}}_{ij} = \dot{\varepsilon}^{\text{p}}_{\text{eq}}\frac{3}{2}\frac{S_{ij}}{\sigma_{\text{eq}}}. \tag{4}$$

In Eq. (4), $S^{\nabla J}_{ij}$ is the Jaumann rate of the stress deviator, G is the shear modulus and $\dot{\varepsilon}^{\text{p}}_{\text{eq}}$ is the equivalent plastic strain rate

$$\dot{\varepsilon}^{\text{p}}_{\text{eq}} = \sqrt{\tfrac{2}{3}D'^{\,\text{p}}_{ij}D'^{\,\text{p}}_{ij}}. \tag{5}$$

In the HJC model, the deviatoric response is determined by the constitutive relation

$$\sigma^*_{\text{eq}} = [A(1-D) + BP^{*N}][1 + C\ln\dot{\varepsilon}^*_{\text{eq}}] \leqslant S_{\max} \quad \text{for } P^* \geqslant 0 \tag{6}$$

in which $\sigma^*_{eq} = \sigma_{eq}/f_c$ is the normalized equivalent stress, $P^* = P/f_c$ is the normalized pressure and $\dot{\varepsilon}^*_{eq} = \dot{\varepsilon}_{eq}/\dot{\varepsilon}_0$ is the normalized strain rate, where $\dot{\varepsilon}_{eq} = \sqrt{\frac{2}{3}D'_{ij}D'_{ij}}$ is the equivalent deviatoric strain rate. The normalizing parameters are the quasi-static uniaxial compressive strength f_c and the reference strain rate $\dot{\varepsilon}_0$. Further, A is the cohesion parameter, B is the pressure hardening coefficient, N is the pressure hardening exponent, C is the strain-rate sensitivity coefficient, and S_{max} is the normalized maximum strength that can be developed. Material degradation is described by the damage variable D, resulting in reduction of the cohesive strength. In the negative pressure regime ($P^* < 0$), the normalized hydrostatic tension $T^* = T/f_c$ is introduced and a linear dependence between the normalized equivalent stress and the normalized pressure is assumed. T is the maximum hydrostatic tension the material can withstand. The original article by HJC [17] does not describe in detail how the point of discontinuity ($P^* = 0$) is treated. The deviatoric response of the HJC model is illustrated in Fig. 2.

The HJC model includes a scalar damage formulation, where the damage evolution is accumulated from both the equivalent plastic strain increment $\Delta\varepsilon^p_{eq}$ (which is caused by plastic shear deformation) and the equivalent plastic volumetric strain increment $\Delta\mu^p_{eq}$ (which is due to plastic crushing of the air voids in the concrete). The damage evolution is expressed as

$$\Delta D = \frac{\Delta\varepsilon^p_{eq} + \Delta\mu^p_{eq}}{\varepsilon^f_p + \mu^f_p}. \tag{7}$$

The plastic strain to fracture $\varepsilon^f_p + \mu^f_p$ is a function of the triaxiality level and is expressed as

$$\varepsilon^f_p + \mu^f_p = \alpha(P^* + T^*)^\beta \geqslant (\varepsilon^f_p)_{MIN}, \tag{8}$$

where α and β are material constants. The lower limit $(\varepsilon^f_p)_{MIN}$ was introduced to allow for a finite amount of plastic strain to fracture the material in order to suppress fracture from low magnitude tensile waves. The compaction response of the HJC model is left to be presented in the next section because a quite similar formulation is adopted in this work, see Fig. 3.

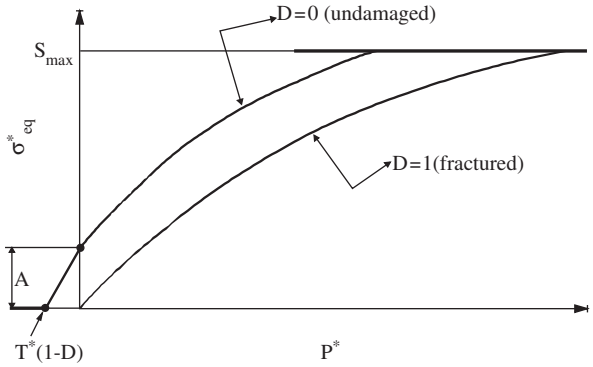

Fig. 2. The shear-pressure strength response of the HJC model.

The theoretical basis of the HJC model is relatively simple and it takes into account most of the important issues of concrete behaviour; namely pressure dependency, rate dependency, damage cracking and compaction (e.g. pressure–volume changes). Other important concrete behaviour mechanisms are not included in the original formulation, for instance the non-linear behaviour before the peak load, the stiffness degradation (Young's modulus reduction), the stiffness recovery (crack closure), the induced anisotropy (loss of isotropy by cracking) and shear reduction influenced by the state of stress (difference between tensile and compressive meridians). It is believed, however, that for impact and penetration applications the compressive waves will reduce the tensile cracking effect caused by the reflected tensile waves by closing them. Consequently, as long as tensile cracking is not considered as the main damage contribution with its correspondent directional effects, the simple isotropic damage formulation seems still attractive (this is not the case for static problems). In addition, the HJC concrete model can be largely improved by introducing the influence of the third stress invariant, hence, differentiating the tensile and compressive meridians.

In order to illustrate the importance of the third invariant, some classical results from the literature [20] related to the experimental behaviour of concrete under static loading conditions are illustrated in Fig. 4. From this figure one can observe the curved shape of the tensile ($\theta = 0^\circ$) and compressive ($\theta = 60^\circ$) meridians, and how the shear capacity increases with increasing pressure. Thus, material models like the HJC model, which only consider the effect of pressure and shear (the latter in terms of the von Mises equivalent stress) in its formulation, will not be able to capture the actual shear variations in the deviatoric plane. For demonstration we include in Fig. 4 the shear strength prediction of the HJC model, using Eq. (6) with $A = 0.75$, $B = 1.65$ and $N = 0.65$ (values commonly used) and excluding both damage and rate effects. Indeed, the HJC model overestimates the shear response for low pressure levels ($P^* < 1$) for both meridians, while the tensile and compressive meridians are overestimated and underestimated, respectively, for higher pressure levels ($P^* > 2$). Based on observations like these a modified version of the HJC model is proposed in the next chapter.

3. The modified HJC (MHJC) constitutive model

3.1. Pressure dependence

In order to avoid the discontinuous description of the original model and consequently circumvent the identification of the cohesion parameter A, the MHJC model adopts a simple continuous function defined by

$$\sigma^*_{eq} = \begin{cases} B[P^* + T^*(1-D)]^N F(\dot{\varepsilon}^*_{eq}) R(\theta, e) \leqslant S_{max} \\ \quad \text{for } P^* \geqslant -T^*(1-D), \\ 0 \quad \text{for } P^* < -T^*(1-D), \end{cases} \tag{9}$$

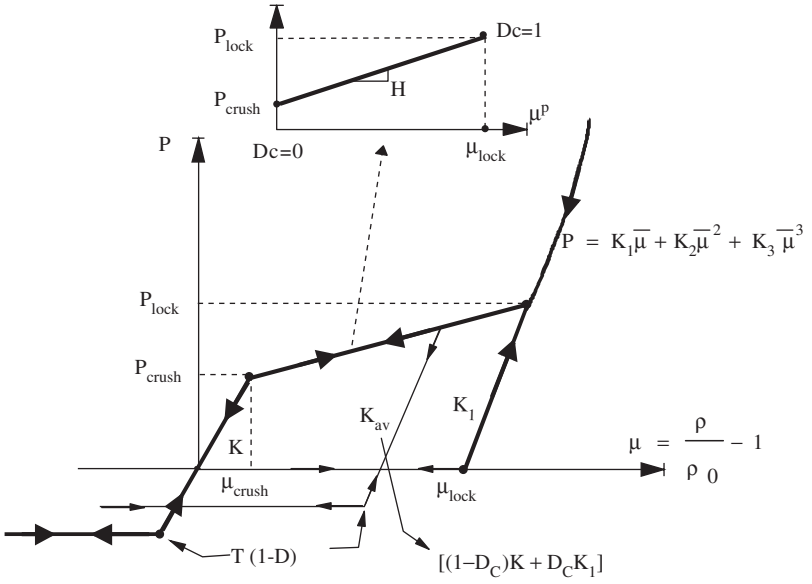

Fig. 3. Pressure–volume response of the HJC concrete model.

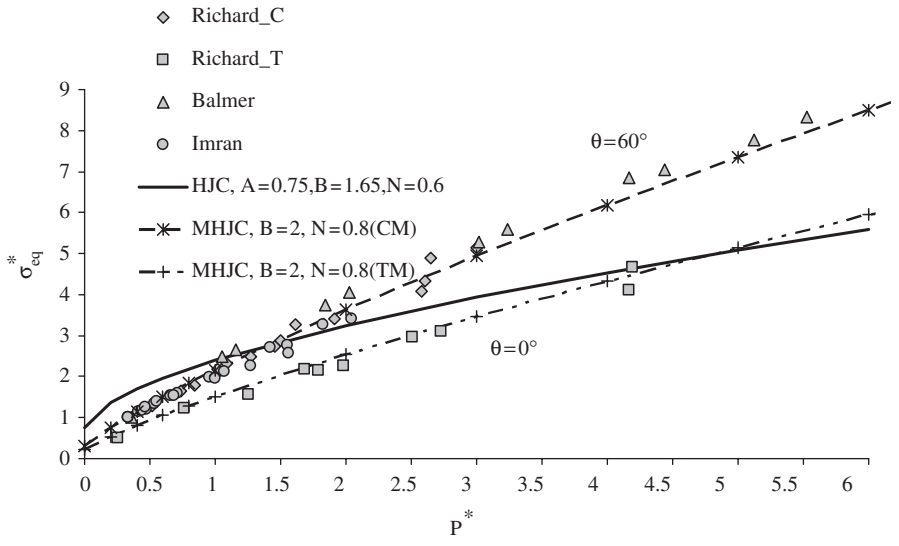

Fig. 4. Experimental concrete shear strength response and MHJC model prediction.

where B, P^*, T^*, N and S_{max} have the same meaning as in the original model, while the new functions $F(\dot{\varepsilon}^*_{eq})$ and $R(\theta, e)$ are defined below. Fig. 4 includes the shear strength prediction of the MHJC model for the compression (CM) and tension meridians (TM) using Eq. (9). For this response values of $B = 2.0$, $N = 0.8$ and a shape factor $e = 0.7$, see Eq. (11), were assumed. Both damage and rate effects were excluded. It is noted that in the MHJC model the normalized cohesive strength is automatically determined by

$$\sigma^*_{eq} = B[T^*(1-D)]^N F(\dot{\varepsilon}^*_{eq}) R(\theta, e) \quad \text{for } P^* = 0. \tag{10}$$

By assuming $1.8 \leqslant B \leqslant 2.0$ and $0.60 \leqslant N \leqslant 0.80$, the MHJC material model agrees with experimental results for the compressive meridian reported in the literature [19]. These results apply for an undamaged state with $D = 0$ and concrete qualities having compressive strengths between 22 and 74 MPa, as illustrated in Fig. 5. Note that it seems to be no experimental evidence of the existence of the shear threshold S_{max}, but this threshold is kept as an option in the MHJC model and is included in Fig. 5 for illustration purposes.

Damage causes a reduction in strength by shifting the maximum strength curve to a damaged state (loss of cohesion), as in the original model. In a complete damaged state with $D = 1$, the concrete behaves as a granular material characterized by a certain residual strength envelop. However, the identification of this residual state is difficult and the authors are not aware of any available information in the literature about the shear behaviour of concrete in a completely damaged state. However, one can assume that the shear capacity in the damage state is

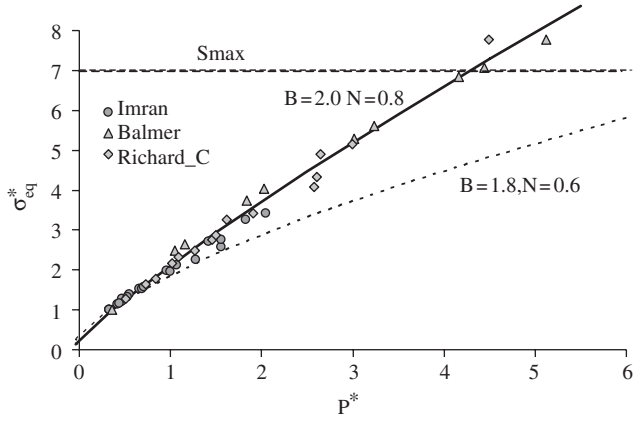

Fig. 5. Undamaged compressive meridian strength response of the MHJC model [19].

reduced by loss of cohesion, i.e. the term $T^*(1-D)$ in Eqs. (9) vanishes.

3.2. Influence of the third shear invariant

Tri-axial experiments on concrete clearly demonstrate the substantial difference of shear strength in conventional tri-axial compression (compressive meridian) and tri-axial extension (tensile meridian) [20]. A reduction of the shear strength on the compressive meridian can be considered by introducing a function R depending on the deviatoric polar angle θ and the normalized out-of-roundness parameter e, as proposed by Willam and Warnke [21], viz.

$$R(\theta,e)=\frac{2(1-e^2)\cos\theta+(2e-1)[4(1-e^2)\cos^2\theta+5e^2-4e]^{1/2}}{4(1-e^2)\cos^2\theta+(1-2e)^2}, \tag{11}$$

where θ is defined as

$$\theta=\frac{1}{3}\cos^{-1}\left(\frac{27|S_{ij}|}{2\sigma_{\mathrm{eq}}^3}\right) \tag{12}$$

in which $|S_{ij}|$ is the determinant of the deviatoric stress tensor S_{ij}. The parameter e is a shape factor that describes the out-of-roundness of the deviatoric trace and it represents the portion of strength on the tensile meridian $\theta=0^\circ$ compared to the state of stress on the compressive meridian $\theta=60^\circ$. The function R is only defined in the sector $0<\theta<\pi/3$, since the polar radius $R(\theta,e)$ extends to all polar directions $0<\theta<2\pi$ using threefold symmetry. Along the tensile and compressive meridian $R(\theta,e)$ takes the values $R(0,e)=e$ and $R(\pi/3,e)=1$, respectively. Convexity and smoothness of this function requires that $0.5<e<1$. The upper limit $e=1$ defines a circle, while the lower limit $e=0.5$ forms a triangle in the deviatoric plane.

The influence of the out-of-roundness parameter e in a plane stress situation was largely commented by Menetrey [22]. He found that the failure envelope is insensitive to the shape factor in the biaxial-tension and tension-compressive regions. However, it strongly affects the biaxial-compression region. The lower limit of the shape factor $e=0.5$ leads to a normalized equi-biaxial compressive strength of 1.0, whereas an upper value of $e=1$ increases dramatically the normalized equi-biaxial compressive strength to 5.3. By adopting the Willam-Warnke concrete model [21], Chen [20] found that the shape factor changes from 0.684 to 0.705 when the pressure goes from 0.33 to 2.33. For moderate pressure levels $1<P^*<3$, Launay and Gauchon [23] reported a shape factor around $e=0.7$. In addition, for high pressure levels a highly ductile behaviour is expected such that the deviatoric shape becomes circular. In order to fit the results of Chen [20] and the classical plane stress experimental results of Kupffer et al. [24] for the biaxial compression case, the following linear function for e in terms of P^* is adopted

$$e=\begin{cases}0.65 & \text{for } P^*<0,\\ 0.65+(1-0.65)\dfrac{P^*}{P^*_{\mathrm{ref}}} & \text{for } 0\leqslant P^*\leqslant P^*_{\mathrm{ref}},\\ 1.0 & \text{for } P^*>P^*_{\mathrm{ref}}.\end{cases} \tag{13}$$

A value of $P^*_{\mathrm{ref}}=10$ was adopted in this work. The reduction factor $R(\theta,e)$ is introduced in a multiplicative way in Eq. (9) as proposed by Riedel [25].

3.3. Rate dependence

In the original HJC concrete model the strain rate influence $F(\dot{\varepsilon}^*)$ is defined as a linear function on a logarithmic scale of the strain rate and characterized by the slope C. However, in order to avoid negative values of $F(\dot{\varepsilon}^*)$ for relative strain rate values $\dot{\varepsilon}^*<1$, while keeping the two-parameter formulation, the following expression proposed by Camacho and Ortiz [26] and largely used by Børvik et al. [27] for metals is adopted, viz.

$$F(\dot{\varepsilon}^*_{\mathrm{eq}})=[1+\dot{\varepsilon}^*_{\mathrm{eq}}]^C, \tag{14}$$

where the parameter C describes the non-linear character of the rate effect. Practically the relative increase in compression strength, found in the literature [28,29], is always related to the static case which involves strain rate values of about $10^{-5}\,\mathrm{s}^{-1}$. For this reason we assumed such a value as the reference strain rate $\dot{\varepsilon}_0$.

3.4. Pressure–volume response

The pressure–compaction response is illustrated in Fig. 3. The pressure P is defined as a function of the volumetric strain

$$\mu=\frac{\rho}{\rho_0}-1, \tag{15}$$

where ρ_0 and ρ are the initial and actual densities, respectively. In compression, the behaviour is divided into three regions. The first region is linear elastic and limited by $(\mu_{\mathrm{crush}},P_{\mathrm{crush}})$. At this state the second region starts, which involves crushing of the concrete and production of

plastic volumetric strains, and it continues until $(\mu_{\text{lock}}, P_{\text{lock}})$. The air voids are then assumed to be fully compressed out of the concrete (compaction damage). In the third region, the concrete is fully dense, i.e. all air voids are removed from the material. The first and second regions are modelled by a classical incremental elasto-plastic-damaging formulation with a linear strain hardening and scalar damage (compaction) assumptions, while the third region is modelled by assuming that concrete is completely elastic (crushed material with no tensile capacity).

In particular, the total volumetric strain increment is separated into its elastic and plastic contributions, according to

$$\Delta\mu = \Delta\mu^{\text{e}} + \Delta\mu^{\text{p}}. \tag{16}$$

The incremental pressure is calculated as

$$\Delta P = H\Delta\mu^{\text{p}}, \tag{17}$$

where the volumetric strain hardening modulus H, see Fig. 3, is defined by

$$H = \frac{P_{\text{lock}} - P_{\text{crush}}}{\mu_{\text{lock}}}. \tag{18}$$

The volumetric plastic strain increment $\Delta\mu^{\text{p}}$ is found with a classical elastic predictor–plastic corrector procedure. Given a total volumetric strain increment $\Delta\mu$, and the previous values of the pressure (P_{i-1}), total (μ_{i-1}) and plastic (μ^{p}_{i-1}) volumetric strains, a trial pressure P_{trial} is calculated assuming an elastic behaviour as

$$P_{\text{trial}} = K_{\text{av}}(\Delta\mu + \mu_{i-1}) = K_{\text{av}}\mu, \tag{19}$$

where the averaged elastic bulk modulus K_{av} is defined according to the compaction damage value (D_{C}, to be defined later) as

$$K_{\text{av}} = (1 - D_{\text{C}})K + D_{\text{C}}K_1. \tag{20}$$

Thus, for a virgin material ($D_{\text{C}} = 0$), $K_{\text{av}} = K$ and for a fully compacted material ($D_{\text{C}} = 1$), $K_{\text{av}} = K_1$. By comparing the pressure in the previous step and the trial calculation one can deduce the incremental volumetric plastic strains according to

$$\Delta\mu^{\text{p}} = \begin{cases} 0 & \text{if } P_{\text{trial}} \leqslant P_{i-1}, \\ \dfrac{P_{\text{trial}} - P_{i-1}}{(K_{\text{av}} + H)} & \text{if } P_{\text{trial}} > P_{i-1}. \end{cases} \tag{21}$$

An updating of the plastic volumetric strain and pressure is done according to

$$\mu^{\text{p}}_i = \Delta\mu^{\text{p}} + \mu^{\text{p}}_{i-1}, \tag{22}$$

$$P_i = K_{\text{av}}(\mu_i - \mu^{\text{p}}_i) = K_{\text{av}}\mu^{\text{e}}_i. \tag{23}$$

The pressure–volume behaviour in the fully compacted region ($P > P_{\text{lock}}$) follows a non-linear elastic behaviour (crushed material with no tensile capacity). For this a modified volumetric strain is introduced

$$\bar{\mu} = \frac{\mu - \mu_{\text{lock}}}{1 + \mu_{\text{lock}}} \tag{24}$$

with

$$\mu_{\text{lock}} = \frac{\rho_{\text{grain}}}{\rho_0} - 1, \tag{25}$$

where ρ_{grain} is the grain density. Replacing Eqs. (15) and (25) into Eq. (24), one gets

$$\bar{\mu} = \frac{\rho}{\rho_{\text{grain}}} - 1 \tag{26}$$

which shows that $\bar{\mu}$ represents the volumetric strain of the aggregate. The behaviour of this material follows a non-linear elastic behaviour of type

$$P = K_1\bar{\mu} + K_2\bar{\mu}^2 + K_3\bar{\mu}^3. \tag{27}$$

This equation is used as long as $D_{\text{C}} = 1$ (fully compacted material). The modified volumetric strain $\bar{\mu}$ is used in the constitutive relation so that the constants K_1, K_2 and K_3 are equivalent to those for a material without voids.

Because no volumetric plastic strains can be generated for tensile (negative) pressures, the elastic predictor scheme works also in this regime. Thus, Eq. (23) can be re-written as

$$P_i = \max(K_{\text{av}}\mu^{\text{e}}_i, -T(1 - D)). \tag{28}$$

Consequently, hydrostatic tension (negative pressure) is always limited by the threshold value of $T(1 - D)$. It is interesting to observe that in the fully compacted zone $D = D_{\text{C}} = 1$, the tensile threshold vanishes (loss of cohesion by complete crushing).

3.5. Damage behaviour

As previously explained, three basic damage mechanisms are always present under impact loading and perforation of concrete materials [12,15,16]. Specifically, tensile cracking (when mode I and II dominate), shear cracking (when mode II and III dominate) and pore compaction are observed. The main idea in this work is to treat each mechanism separately, and for this purpose three internal damage variables D_{T}, D_{S} and D_{C}, representing the tensile, shear and compaction damage, respectively, need to be introduced.

3.5.1. Tensile damage (brittle cracking)

Tensile cracking is the main source of non-linearity in concrete and is due to concrete's low strength in tension when compared to compression. Therefore, concrete structures include some kind of reinforcement (commonly steel) in these zones where tensile stresses are expected. Prediction of tensile cracking has been largely studied and basically three types of models are commonly used: the fictitious crack model [30], the smeared crack approach [31] and the damage mechanics based models [13,15,16]. In these models the introduction of a crack formation

criterion is required. Two of the most popular crack formation criteria are the Rankine criterion that is based on the maximum principal stress and the Saint Venant criterion that is based on the maximum principal strain. Alternatively, a critical hydrostatic tension or a critical hydrostatic tensile strain can be considered as a fracture criterion. Without putting too much effort on deciding which criterion predicts the crack pattern best, it was decided to use the hydrostatic tensile strain as the main indicator for crack formation. For this, the minimum value of the volumetric strain μ (in the tensile regime) attained during the loading history is assumed as the equivalent strain for crack formation and it reads

$$\varepsilon_{\mathrm{T}}^{t} = \min(\varepsilon_{\mathrm{T}}^{t-1}, \min(0, \mu^{t})), \tag{29}$$

where the superscripts t and $t-1$ indicate the actual and previous increment, respectively. The tensile damage criterion is simply defined by

$$D_{\mathrm{T}} = \begin{cases} 0 & \text{for } \varepsilon_{\mathrm{T}}^{t} > \varepsilon_{0}, \\ 1 & \text{for } \varepsilon_{\mathrm{T}}^{t} \leqslant \varepsilon_{0}, \end{cases} \tag{30}$$

where $\varepsilon_0 = -f_{\mathrm{t}} F(\dot{\varepsilon}_{\mathrm{eq}}^{*})/K$ is the volumetric tensile strain threshold for crack formation. The factor $F(\dot{\varepsilon}_{\mathrm{eq}}^{*})$, see Eq. (14), is included to take into account the strain rate effect in the tensile regime. When dealing with reinforced concrete and penetration problems, tensile cracking is assumed to be less important than shear cracking. Thus, the damage variable D_{T} is used only as a tensile damage indicator, i.e. it has no influence on the stress–strain behaviour and is used only for post-processing purposes.

3.5.2. Shear damage

The cumulative damage development proposed in the HJC original model [17] is adopted here, but damage from shear and volumetric straining is separated. The evolution of the shear damage variable D_{S} is defined by

$$\Delta D_{\mathrm{S}} = \frac{\Delta \varepsilon_{\mathrm{eq}}^{\mathrm{p}}}{\varepsilon_{\mathrm{p}}^{\mathrm{f}}}. \tag{31}$$

The plastic strain to fracture $\varepsilon_{\mathrm{p}}^{\mathrm{f}}$ is here adopted in the form

$$\varepsilon_{\mathrm{p}}^{\mathrm{f}} = \alpha[P^{*} + T^{*}]^{\beta} \geqslant (\varepsilon_{\mathrm{p}}^{\mathrm{f}})_{\mathrm{MIN}}, \tag{32}$$

where α and β are constants (as in the original model). It transpires that the plastic strain to fracture $\varepsilon_{\mathrm{p}}^{\mathrm{f}}$ increases as P^{*} increases. The third damage constant $(\varepsilon_{\mathrm{p}}^{\mathrm{f}})_{\mathrm{MIN}}$ is introduced to allow for a finite amount of plastic strain to fracture the material.

3.5.3. Compaction damage

Damage compaction due to plastic volumetric strain is included in the equation of state defined by the Pressure–volume law. Two consequences should be taken into account with this mechanism: the cohesive strength of the concrete is lost during air voids collapse (i.e. the pore compaction contributes to damage) and the bulk stiffness increases (i.e. the bulk modulus approaches to that of a compacted material). Thus, an internal compaction damage variable D_{C} can be defined as

$$\Delta D_{\mathrm{C}} = \frac{\Delta \mu^{\mathrm{p}}}{\mu_{\mathrm{lock}}}. \tag{33}$$

Here, $\Delta\mu^{\mathrm{p}}$ is the incremental plastic volumetric strain (defined by Eq. (21)) and μ_{lock} is the plastic volumetric strain of the fully compacted granular material (an input parameter). It should be pointed out that the compaction damage variable introduced in this work agrees with the interpolation factor F defined in the original HJC model [17,18].

3.5.4. Total damage

The combination of three different damage mechanisms, defined by the damage variables D_{T}, D_{S} and D_{C}, into one representative scalar value D is questionable. However, it is believed that by including only D_{S} and D_{C} in the averaging procedure, reasonable results can still be obtained. This proposal is based on the fact that for moderate and high confining pressure levels both D_{S} and D_{C} describe the "ductile" behaviour of concrete and in this way a shear strength reduction in Eq. (9) by void collapse can be included. A similar averaging procedure was proposed in [25]. The total damage effect is calculated here as

$$(1 - D) = \sqrt{(1 - D_{\mathrm{S}})(1 - D_{\mathrm{C}})}. \tag{34}$$

Still under the framework of the scalar damage theory the exclusion of D_{T} in the averaging proposal of Eq. (34) is based on the argument that the tensile cracking effect is reduced by the presence of the steel reinforcement (if present) and the competition between crack closure and opening caused by the compressive and tensile waves propagation.

4. Behaviour of the MHJC model

The MHJC concrete model has been implemented in the finite element code LS-DYNA [7] and this section presents a description of the parameter identification and some numerical tests performed to verify the numerical implementation and the sensitivity of some of the parameters. The model requires the identification of 19 parameters: the initial density ρ_0; the two elastic constants E (Young's modulus) and ν (Poisson's ratio); five shear-pressure strength constants defined by the uniaxial compressive (f_{c}) and tensile (f_{t}) strengths, the hardening coefficient (B), the hardening exponent (N) and the maximum shear strength ($S_{\max}$); two rate sensitivity parameters ($\dot{\varepsilon}_0$, C); three damage constants to define the softening behaviour ($\alpha, \beta, (\varepsilon_{\mathrm{p}}^{\mathrm{f}})_{\mathrm{MIN}}$); and seven constants to describe the pore compaction behaviour where the elastic region is defined by P_{crush} and μ_{crush}, the crushing region by P_{lock} and μ_{lock}, and K_1, K_2 and K_3 define the behaviour of a fully compacted material. In the next section we present the tests required and calibration procedure for the model parameters identification.

The sensitivity of the strength parameters was analysed for the uniaxial and biaxial compressive tests, because they are placed at the two extreme meridians; namely the compressive meridian ($\theta = 60^\circ$) for the first case and the tensile meridian ($\theta = 0^\circ$) for the second case. The possibility to obtain different softening responses in a uniaxial compressive test is illustrated by the adequate choice of the damage parameters. The pressure–volume law is described with the classical hydrostatic state of stress and, finally, the influence of the lateral confining pressure is illustrated when comparing the response of the uniaxial compressive strain vs. the uniaxial compressive stress.

4.1. Uniaxial compression ($\theta = 60^\circ$)

The following example illustrates the sensitivity of the MHJC model to the shear strength parameters. For this purpose a uniaxial compression test (compression meridian) is used. The pressure–volume behaviour is assumed linear elastic and damage is inhibited (i.e. $(\varepsilon_p^f)_{MIN} = 1.0$). The strain rate effect is not included. Typical values of $B = 2.0$ and $N = 0.75$ are assumed, see Section 3. Considering a uniaxial compressive and tensile strength value of $f_c = 43\,\text{MPa}$ and $f_t = 2.4\,\text{MPa}$, respectively, Eq. (9) yields $\sigma^*_{eq} = 0.985$, or in other words, the uniaxial compressive strength input f_c is practically recovered. In the original model, the set of parameters $A = 0.75$ (i.e. the cohesive strength), $B = 1.6$ and $N = 0.75$ is frequently assumed [17,24]. However, with such values in Eq. (6) the uniaxial compressive strength is overestimated by about 45%. In the modified version presented here, the cohesive strength is calculated automatically and the uniaxial compressive strength is in general recuperated. Fig. 6 illustrates the main result of this analysis.

4.2. Bi-axial compression ($\theta = 0^\circ$)

The following example is for biaxial compression (tensile meridian) where the influence of the strength parameter B (i.e. the shear strength dependence on the meridian) is studied. In [12], it was concluded that in the original HJC a value of $B = 1.2$ seems more adequate to characterize the tensile meridian, while a value of $B = 2.0$ was appropriated

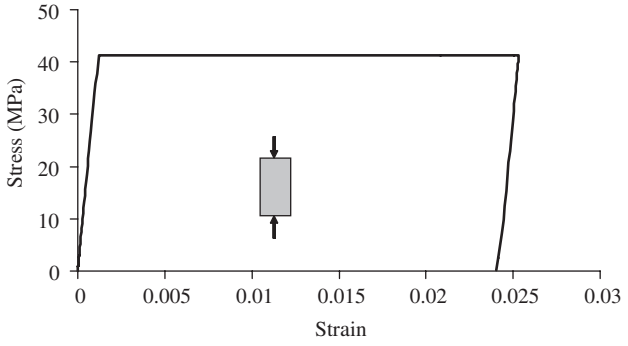

Fig. 6. Uniaxial compressive ($\theta = 60^\circ$) response of the MHJC model.

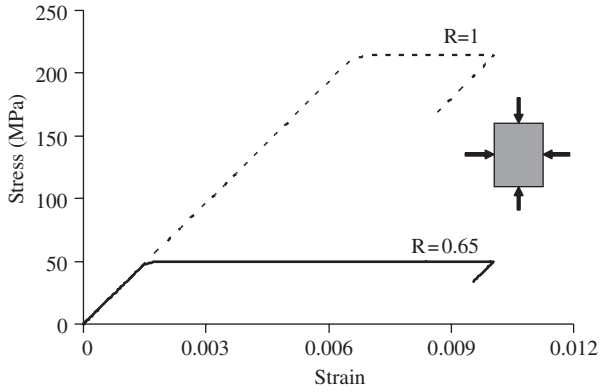

Fig. 7. Biaxial compressive ($\theta = 0^\circ$) response of the MHJC model.

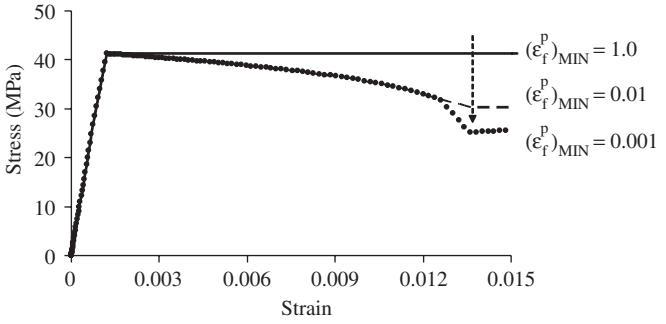

Fig. 8. Influence of damage parameter $(\varepsilon_p^f)_{MIN}$ on the softening behaviour.

to characterize the compressive meridian. However, it was pointed out that the HJC model was limited to select an adequate value B representing a good compromise for both meridians at the same time. This compromise is relaxed in the modified version by including the reduction effect of the third shear invariant through the function $R(\theta, e)$. The numerical result of the biaxial compressive test is illustrated in Fig. 7, where the influence of $R(\theta, e)$ is clearly observed. Indeed, a prediction of about five times the uniaxial compressive strength is obtained when $R(\theta, e)$ equals unity (i.e. a circular shape of the deviatoric trace), while an increase of only 20% of the uniaxial compressive strength is seen when $R(\theta, e) = 0.65$ (i.e. more triangular shape of the deviatoric trace). This result agrees well with the experimental findings of Kupffer et al. [24].

4.3. Strain softening response

Fig. 8 illustrates the different softening responses for a uniaxial compression test predicted by the MHJC model. Here, values of $\alpha = 0.04$ and $\beta = 1$ were assumed. The softening response shows the influence of the fracture strain threshold $(\varepsilon_p^f)_{MIN}$, see Eq. (32), on the residual strength. As one can see, the residual stress is reduced when this parameter is increased. Larger values of $(\varepsilon_p^f)_{MIN}$ delay damage development.

The slope of the softening response is affected by the parameters α and β in Eq. (32), and the softening response is most sensitive to the exponent β. The influence of this

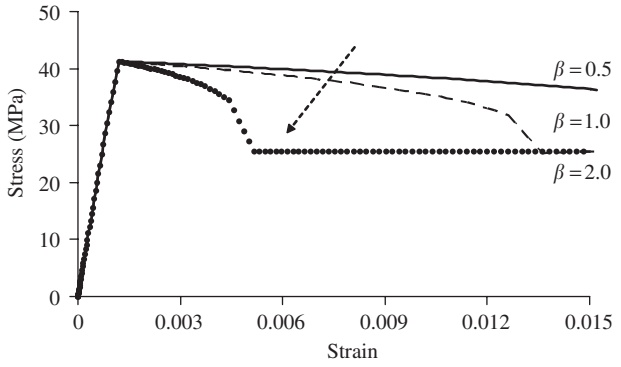

Fig. 9. Influence of damage parameter β on the softening behaviour.

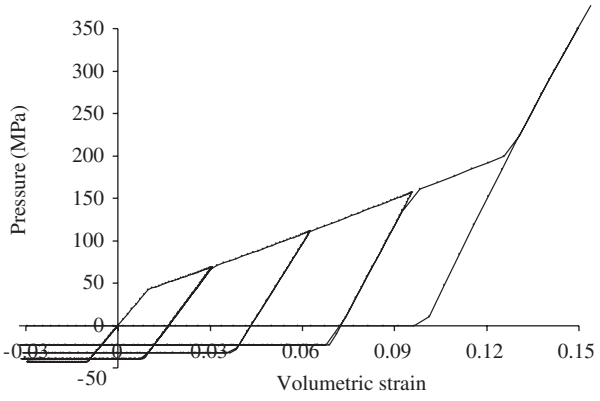

Fig. 10. Pressure–volume response of the MHJC concrete model.

parameter for a uniaxial compression test is illustrated in Fig. 9 where values of $(\varepsilon_p^f)_{MIN} = 0.001$ and $\alpha = 0.04$ were assumed.

4.4. Cyclic hydrostatic pressure

This example describes the response of the MHJC concrete model under an alternating hydrostatic state of stress. The pore-compaction behaviour adopted follows the original formulation of the HJC concrete model. Note that the main parameters involved are chosen for illustration purposes and can deviate from representative values for actual concrete materials. The compressive and tensile strengths are assumed to be the same ($f_c = f_t = 43$ MPa). The elastic pressure–volume region is defined by $P_{crush} = 43$ MPa and $\mu_{crush} = 0.01$ (this involves a bulk modulus of $K = 4300$ MPa). The "plastic region" is bounded by $P_{lock} = 200$ MPa and $\mu_{lock} = 0.10$. The fully compacted material is described by the three constants $K_1 = 8500$ MPa, $K_2 = -17\,100$ MPa and $K_3 = 20\,800$ MPa taken from the original paper. The cyclic pressure–volume response is illustrated in Fig. 10.

4.5. Influence of the confining pressure

It is well known that for metals the yield properties are quasi-independent of the hydrostatic pressure, contrary to geo-materials. Indeed, pressure-dependent materials like concrete are characterized by its shear strength increase with an increasing pressure. The positive effect of the confining pressure on shear strength is illustrated in Fig. 11 by comparing two extreme loading situations: the classical uniaxial stress (with no lateral confinement) versus the uniaxial strain situation (varying high lateral pressure to allow only vertical displacements). This result is qualitatively in agreement with the expected response for concrete materials.

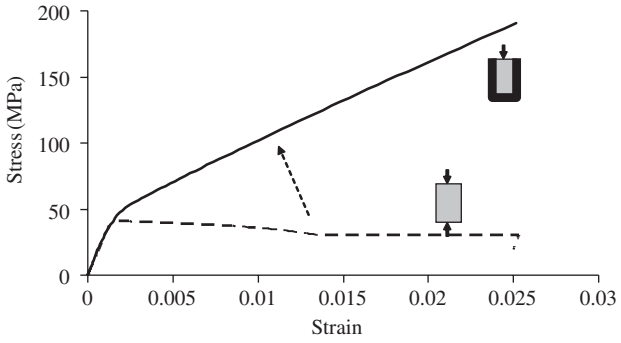

Fig. 11. Uniaxial compression versus uniaxial strain response; influence of lateral pressure.

5. Parameter identification

As previously indicated the MHJC concrete model requires the identification of 19 parameters. The required tests and calibration procedure for a complete identification of the material parameters involved are:

(a) Uniaxial compression test for identification of E, v, ρ_0 and f_c.
(b) Uniaxial tensile test for identification of T (using the tensile strength f_t).
(c) Triaxial compression tests with varying confinement pressures to identify B, N and S_{max}.
(d) Hydrostatic compression test to identify the Pressure–volume response defined by the following set of parameters: P_{crush}, μ_{crush}, P_{lock}, μ_{lock} and K_1, K_2, K_3.
(e) The damage parameters α and β can be identified from fracture strain curves for different pressure levels (triaxiality effect). Hence, fracture strain values from tests proposed in (a) and (c) can be used to calibrate the damage parameters. The fracture strain threshold $(\varepsilon_p^f)_{MIN}$ is more difficult to identify. However, to avoid fracture from low magnitude tensile stress the values, $(\varepsilon_p^f)_{MIN}$ can be assumed as the fracture strain of a uniaxial compression test.
(f) Finally, the rate sensitivity parameters $\dot{\varepsilon}_0$ and C require uniaxial compression tests for different strain rate levels.

It is believed that among the most important issues when developing mathematical models for the characterization of materials behaviour one should address, first, the compromise between accuracy and simplicity and, second,

the compromise between the material parameters and tests required for identification. At first, a complete calibration of the parameters involved in MHJC seems complex and expensive, because one needs the stress–strain curve to failure in uniaxial compression and at least two triaxial compression tests with different confining pressure levels. From these three tests E, ν, ρ_0, f_c, B, N, α, β and $(\varepsilon_p^f)_{MIN}$ can be identified. There is no experimental evidence of the existence of a shear strength threshold (S_{max}), and if it does exist its identification could demand extremely high lateral pressure levels. Therefore, in this study the shear strength threshold will be given a high value, $S_{max} \geqslant 7$, as is commonly assumed in the literature [17,18]. Next, the splitting test can be used to identify the tensile strength f_t. Furthermore, the pressure–volume law can in principle be extracted from one hydrostatic compression test. However, the complete representation of this law will require extremely high pressures, rendering difficult the identification of the parameters P_{lock}, μ_{lock} and (K_1, K_2, K_3). Finally, at least three uniaxial compression tests with different strain rates should be performed for identification of the rate sensitivity parameters $\dot{\varepsilon}_0$ and C.

As a result, a total of eight tests (i.e. five uniaxial and three triaxial tests) are needed for the complete identification of the parameters required in the MHJC concrete model. Another valid alternative consists of including a smaller number of tests complemented with inverse modelling and assumptions related to some values. For instance, the material strength characterization requires the uniaxial compressive strength f_c and the initial density ρ_0, while the uniaxial tensile strength f_t can be related to the compressive strength, i.e. $f_t = 0.54\sqrt{f_c}$, according to the FIB/CEB [32]. Also Young's modulus E can be related to the compressive strength, i.e. $E = 11\,700(f_c)^{0.3}$ [33]. A Poisson's ratio of $\nu = 0.2$ can be assumed. The shear-pressure behaviour can be represented by assuming values of $1.8 \leqslant B \leqslant 2.0$ and $0.60 \leqslant N \leqslant 0.80$ according to the experimental results in the compressive meridian presented in the literature [19]. In these results concrete qualities between 22 and 74 MPa compressive strengths were reported. It should be pointed out that "special" concretes can deviate largely from the B and N values previously proposed. As a matter of fact, in the experimental program on perforation of concrete slabs, conducted by Hanchak et al. [34], two concrete qualities C_48 and C_140 with special glassy gravel (called Steilacoon Glacial) were used. The hardness of this type of gravel is slightly lower than a quartz mineral type. The shear-pressure response of a series of triaxial tests reported in Hanchak et al. [34] is illustrated in Fig. 12. By a fitting procedure one finds values of $B = 1.4$, $N = 0.65$ and $B = 1.30$, $N = 0.45$ for the concrete qualities of C_48 and C_140, respectively, hence invalidating the proposed B and N values for "normal" concretes. To sum up, two triaxial compression tests would be preferable for accurate identification of B and N. Next, some of the parameters involved in the pressure–volume law can easily be identified. For instance, from elasticity

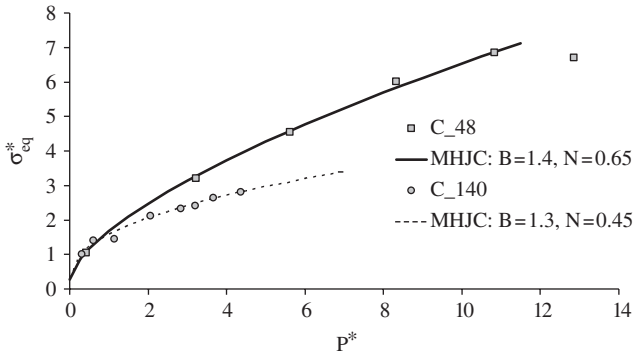

Fig. 12. Shear-pressure response reported by Hanchak et al. [34] and the identification of B and N parameters used in the MHJC concrete model.

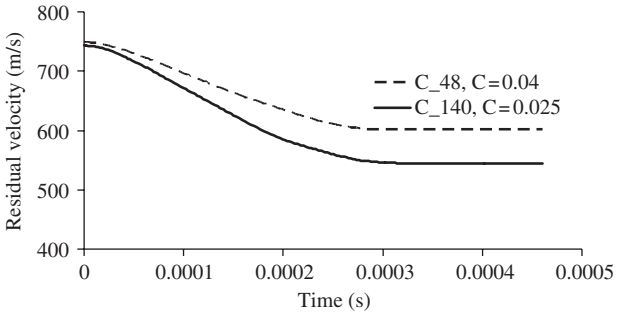

Fig. 13. Identification of the rate sensitivity parameter C by inverse modelling.

$P_{crush} = f_c/3$ and $\mu_{crush} = f_c(1-2\nu)/E$, while μ_{lock} can be assessed from the density of the gravel material (ρ_{grain}) and the initial density of concrete (ρ_0) using $\mu_{lock} = \rho_{grain}/\rho_0 - 1$. Unfortunately, the identification of P_{lock} and (K_1, K_2, K_3) requires hydrostatic tests at very high pressure levels. It is believed, based on results in the literature [17,18], that $P_{lock} \geqslant 600$ MPa and $K_1 = 8500$ MPa, $K_2 = -17\,100$ MPa and $K_3 = 20\,800$ MPa are representative values for concrete materials. In order to avoid the identification of ductility diagrams (fracture strain versus triaxiality), values of $\alpha = 0.04$ and $\beta = 1.0$ can be assumed to represent the concrete damage behaviour with reasonable accuracy [17,18]. The fracture parameter $(\varepsilon_p^f)_{MIN}$ with values of 0.01 (low strength quality) and 0.005 (high strength quality) can be introduced to represent different embrittlement characteristics.

In the original paper [17] the strain rate effect was assumed to be independent of the concrete strength, while there is experimental evidence that high strength concretes are less sensitive to variation in strain rates than conventional ones [28,29]. Based on this argument it was decided to use inverse modelling in the high impact velocity region (i.e. from 500 to 1000 m/s) to identify the rate sensitivity parameter C. In the inverse modelling procedure we identify the C value which gives the best numerical fit (e.g. residual velocity) to one experimental point and use it to predict the entire residual velocity diagram. With this

procedure values of $C = 0.04$ for the C_48 concrete and $C = 0.025$ for C_140 concrete were found based on the penetration results reported by Hanchak et al. [34]. Indeed, for the C_48 concrete slab an experimental residual velocity of 602 m/s was found when the impact velocity was 749 m/s while for the C_140 concrete slab with an impact velocity of 743 m/s an experimental residual velocity of 545 m/s was found. By using the MHJC concrete model in the numerical simulations these values were practically recuperated (615 and 544 m/s), as illustrated in Fig. 13.

6. Numerical simulation of perforation of concrete slabs

6.1. Experimental study by Hanchak et al. [34]

The ballistic limit computations are based on the test performed by Hanchak et al. [34], where square reinforced concrete plates of $610 \times 610 \times 178\,\text{mm}^3$ were tested. Three layers of square-pattern reinforcement steel rods with a diameter of 5.6 mm were used. Two concrete qualities C_48 and C_140 with uniaxial compressive strength $f_c = 48$ and 140 MPa, and uniaxial tensile strength $f_t = 4$ and 5 MPa, respectively, were used. In addition to the pressure–compaction curves, triaxial tests were performed under various confining pressure levels such that shear strength versus pressure curves could be established, see Fig. 12. A 30-mm, smooth-bore powder gun was used to launch 0.50 kg ogival-nose steel projectiles with a length of 143.7 mm and a diameter of 25.4 mm. In the tests, initial and residual projectile velocities were measured. These values were used to construct initial versus residual velocity curves for the two concrete qualities and from these diagrams ballistic limits were deduced. Hanchak et al.'s main conclusion was that even though the unconfined compressive strength was increased by a factor of three, the ballistic limit velocity only increased by 20%. This is due to the fact that the shear strength ratios of the two concrete materials studied approach each other for relatively small confining pressures.

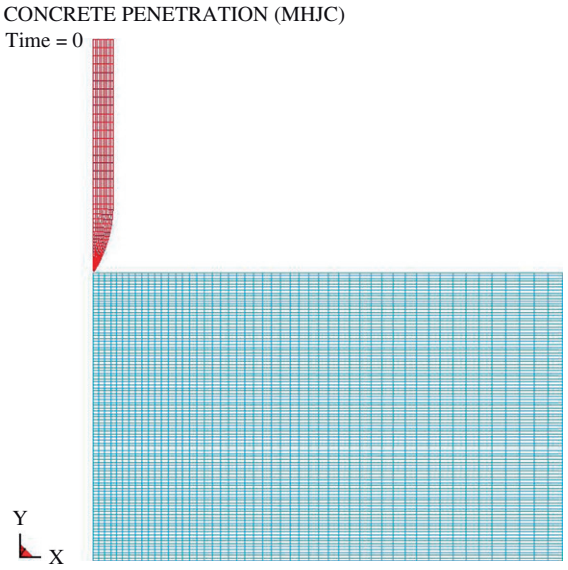

Fig. 14. 2D axisymmetric finite element model used in the penetration analysis (target radius is 305 mm and target thickness is 178 mm).

6.2. Concrete slabs with $f_c = 48$ MPa

Finite element analyses with 2D axisymmetric elements were performed. A reduced integration scheme with hourglass control was adopted. The finite element model is illustrated in Fig. 14. For the concrete slab a total of 100 elements were used through the thickness and 50 elements along the radius. The steel reinforcement was not included in the simulations since the effect on the perforation resistance was found negligible [34]. The set of input parameters assumed in the simulations are indicated in Table 2. The steel projectile was modelled using a von Mises material model (Mat_003 in LS-DYNA) with linear isotropic hardening. The main data used for the projectile are $E = 200$ GPa, $\nu = 0.3$, $\sigma_Y = 1.72$ GPa and $E_T = 15.0$ GPa (tangent modulus). No strain rate effect was considered. The original density of the projectile ($8020\,\text{kg/m}^3$) was slightly modified to $8300\,\text{kg/m}^3$ to obtain the total launch package mass of 0.53 kg. In the present calculations, we adopted the element erosion option of LS-DYNA with a criterion based on the maximal principal strain with a failure strain value of $(\varepsilon_1)_{MAX} = 1.0$ (based on similar values used in [18]). The 2D_automatic_single_surface contact option of LS-DYNA was used to define the contact behaviour between steel and concrete without friction. The rate sensitivity parameter value of $C = 0.04$ was used based on the residual velocity predictions of Section 5. The number of elements used in this study, i.e.

Table 2
Material parameters for concrete with $f_c = 48$ MPa

ρ_0 (kg/m^3)	E (MPa)	ν	B	N	C	S_{max}
2440	$11\,700\,(f_c)^{0.3}$	0.2	1.4	0.65	0.04	7
f_c (MPa)	f_t (MPa)	$\dot{\varepsilon}_0$ (s^{-1})	α	β	$(\varepsilon_p^f)_{MIN}$	
48	4	1×10^{-5}	0.04	1.0	0.01	
P_{crush} (MPa)	μ_{crush}	P_{lock} (MPa)	μ_{lock}	K_1 (MPa)	K_2 (MPa)	K_3 (MPa)
16	$f_c(1-2\nu)/E$	800	0.1	8500	−17 100	20 800

100 elements over the target thickness, was similar to that used in the original paper by HJC [17]. However, the influence of the mesh size, mesh bias, friction effects and erosion strain parameters are not included in this work. These issues will be considered in a forthcoming study.

The numerical predictions of the residual velocity are compared with the experimental findings [34] for the C_48 concrete in Fig. 15. The MHJC compares very well with the experimental values, in particular for impact velocities higher than 400 m/s. The predicted ballistic limit (325 m/s) deviates by less than 5% from the experimental value (340 m/s). The tensile damage (cracking) evolution during the perforation process is illustrated in Fig. 16.

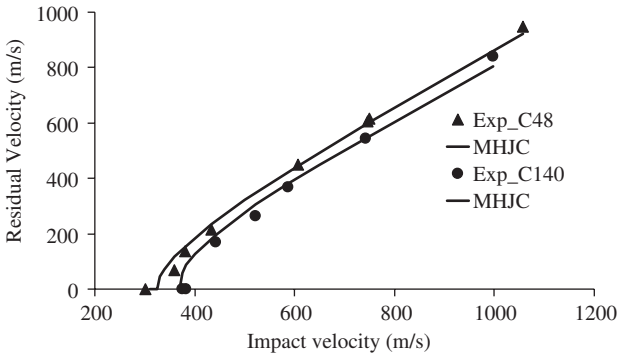

Fig. 15. Ballistic limit predictions using the MHJC for C_48 and C_140 concrete qualities.

6.3. Concrete slabs with $f_c = 140$ MPa

The uniaxial compressive and tensile strength of this concrete was $f_c = 140$ and $f_t = 5$ MPa, respectively. A new set of input parameters based on the tests performed by Hanchanck et al. [34] is compiled in Table 3. We used the material data of the previous example for the projectile. The element erosion option with a failure strain value of $(\varepsilon_1)_{MAX} = 1.0$ and the 2D_automatic_single_surface contact option without friction of LS-DYNA were once again adopted. A rate sensitivity parameter value of $C = 0.025$ was found for this case (see Section 5). In addition, the plastic fracture strain limit is reduced to $(\varepsilon_p^f)_{MIN} = 0.004$ in order to account for the brittle nature of high strength concrete. The numerical predictions of residual velocity are compared with the experimental findings [34] in Fig. 15. Also in this case the MHJC compares well with the experiments, and the predicted ballistic limit (370 m/s) deviates by less than 8% from the experimental one (400 m/s).

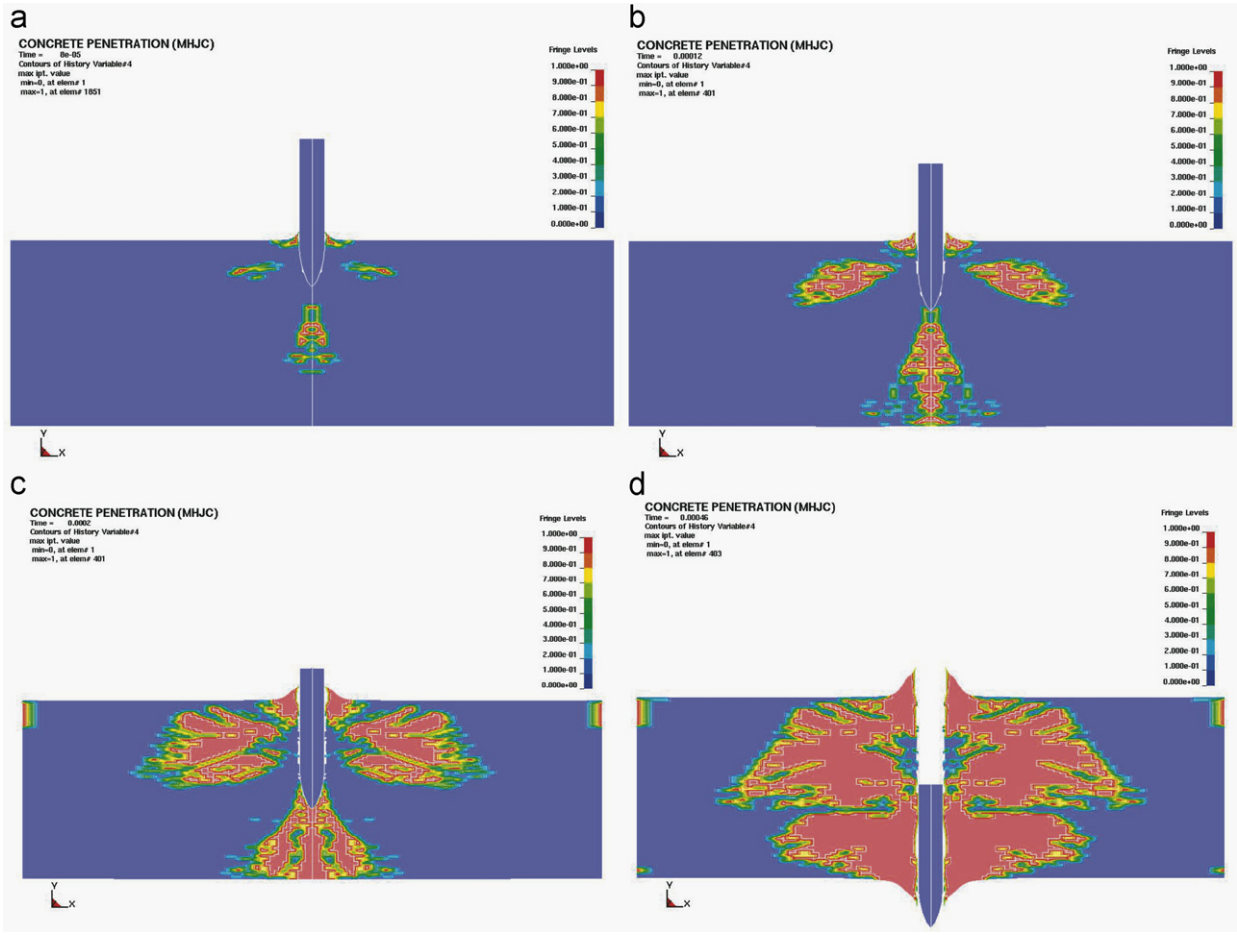

Fig. 16. Tensile damage development during perforation of the C_48 concrete slab.

Table 3
Material parameters for concrete with $f_c = 140$ MPa

ρ_0 (kg/m^3)	E (MPa)	v	B	N	C	S_{max}
2520	11 700 $(f_c)^{0.3}$	0.2	1.30	0.45	0.025	7
f_c (MPa)	f_t (MPa)	$\dot{\varepsilon}_0$ (s^{-1})	α	β	$(\varepsilon_p^f)_{MIN}$	
140	5	1×10^{-5}	0.04	1.0	0.004	
P_{crush} (MPa)	μ_{crush}	P_{lock} (MPa)	μ_{lock}	K_1 (MPa)	K_2 (MPa)	K_3 (MPa)
46	$f_c(1-2v)/E$	800	0.04	8500	−17 100	20 800

6.4. Discussions

Both the original and the modified version of the HJC model are able to reproduce the experimental findings of the penetration tests of Hanchak et al. [34]. It is believed that during the penetration process the energy dissipated (dominated by shear damage) in the original HJC model is of similar magnitude of that predicted by the MHJC model. So if the normalized pressure levels generated in the slabs during the penetration test are ranging between 1 and 5 the shear response of the HJC represent an averaged response of the MHJC model, see Fig. 4. However, large differences between these models are expected if the normalized pressures in the target are less than 1 (thin slabs) or larger than 5 (massive blocks). On the other hand, our predictions are in agreement with both concrete qualities used by Hanchak et al. [34]. To this end, the enhancements proposed to the original HJC concrete model show more consistency with classical uniaxial compression and biaxial static tests reported in the literature, eliminate the cohesive parameter (difficult to identify), introduce classical observed damage mechanisms. Further, the inverse modelling procedure used to identify the strain rate parameter allows capturing the influence of the concrete quality. The proposed modifications are expected to improve the numerical predictions of the original version.

7. Concluding remarks

The Holmquist–Johnson–Cook (HJC) model for concrete materials subjected to impact loading has been investigated in the current study, and some modifications are proposed to the pressure-shear behaviour, the strain-rate sensitivity term and the damage description. A critical review of the constitutive model with alternative proposals for parameter identification is provided. Ballistic limit assessments with deviations under 8% were found when compared to experimental results from the literature, indicating that the MHJC model represents a good compromise between simplicity and accuracy for large-scale computations of concrete plates impacted by projectiles.

Acknowledgements

The authors gratefully acknowledge the financial support of the Department of Applied Mechanics and Corrosion at SINTEF, Materials and Chemistry and The Norwegian Defence Estates Agency, Research & Development Department.

References

[1] Corbett GG, Reid SR, Johnson W. Impact loading of plates and shells by free-flying projectiles: a review. Int J Impact Eng 1996; 18(2):141–230.
[2] Børvik T, Langseth M, Hopperstad OS, Polanco-Loria MA, Ballistic perforation resistance of high performance concrete slabs with different unconfined compressive strengths. In: Brebbia CA, de Wilde WP, editors. Proceedings of first international conference on high performance structures and composites. Sevilla, Spain: WIT press (ISBN 1-85312-904-6); 2002. p. 273–282.
[3] Kennedy RP. A review of procedures for the analysis and design of concrete structures to resist missile impact effects. Nucl Eng Design 1976;37:183–203.
[4] Ben-Dor G, Dubinsky A, Elperin T. Ballistic impact: recent advances in analytical modeling of plate penetration dynamics—a review. Appl Mech Rev 2005;58:355–71.
[5] Li QM, Reid SR, Wen HM, Telford AR. Local impact effects of hard missiles on concrete targets. Int J Impact Eng 2005;32:224–84.
[6] Abaqus v 6.2 User's Manual Hibbitt, Karlsson and Sørenson Inc. Providence, RI, USA, 2001.
[7] LS-DYNA Keyword User's Manual Ver. 950, Livermore Software Technology Corporation, LSCT, 1999.
[8] AUTODYN, Theory Manual, Century Dynamics Ltd. Horsham, England, 1997.
[9] Teng TL, Chu YA, Chang FA, Chin HS. Numerical analysis of oblique impact on reinforced concrete. Cement Concr Compos 2005;27:481–92.
[10] Leppänen J. Concrete subjected to projectile and fragment impacts: modelling of crack softening and strain rate dependency in tension. Int J Impact Eng 2006;32:1828–41.
[11] Tai YS, Tang CC. Numerical simulation: the dynamic behaviour of reinforced concrete plates under normal impact. Theor Appl Fract Mech 2006;45:117–27.
[12] Polanco-Loria M. Constitutive models for concrete materials under impact loading conditions. SINTEF Report STF24 F00315, Trondheim, Norway, 2001.
[13] Polanco-Loria M. Numerical modelling of plain and reinforced concrete by damage mechanics. PhD dissertation, The Norwegian Institute of Technology, Norway, 1997.
[14] Isenberg J, editor. Finite element analysis of reinforced concrete structures II. Proceedings of the international workshop sponsored by

the U.S. National Science Foundation, Defence Nuclear Agency and the U.S. Army Corps of Engineers. New York, USA: ASCE; 1991.
[15] Mazars J. Application de la mecanique de l'endommagement au comportement nonlineaire et la rupture du beton de structure, These de Doctorate d'Etat, LMT, Universite de Paris, France, 1984.
[16] Burlion N. Compaction des betons: elements de modelisation et caracterisation experimentale. PhD dissertation, LMT, ENS de Cachan, France, 1997.
[17] Holmquist TJ, Johnson GR, Cook WH. A computational constitutive model for concrete subjected to large strains, high strain rates and high pressures. In: Proceedings of 14th international symposium on Ballistics, Quebec, Canada, 1993. p. 591–600.
[18] Johnson GR, Beissel SR, Holmquist TJ, Frew DJ. Computer radial stresses in a concrete target penetrated by a steel projectile. In: Jones N, Talaslidis DG, Brebbia CA, Manolis GD, editors. Proceedings of structures under shock and impact V, held at the Aristotle University of Thessaloniki, Greece (ISBN:1853125903). Southampton, UK: Computational Mechanics Publications; 1998. p. 793–806.
[19] Polanco-Loria M. Improvements to the HJC concrete model in LS-DYNA SINTEF Report STF24 F01286, Trondheim, Norway, 2002.
[20] Chen WF. Plasticity in reinforced concrete. New York: Mc Graw Hill; 1982.
[21] Willam KJ, Warnke EP. Constitutive model for the triaxial behaviour of concrete. In: International association of bridges and structural engineers, seminar on concrete structures subjected to triaxial stresses, Paper III-1, IABSE Proceedings 19, Bergamo, Italy, 1975.
[22] Menetrey P. Numerical analysis of punching failure in reinforced concrete structures. PhD dissertation, Ecole Polytechnique Federale de Lausanne, Switzerland, 1994.
[23] Launey P, Gachon H. A study of the failure of concrete under combined compressive stress. University of Illinois, Engineering Experimental Station, Bulletin No. 185, 1970.
[24] Kupffer H, Hilsdorf H, Rush H. Behaviour of concrete under biaxial stresses. ACI J 1969;23:656–65.
[25] Riedel W. Ein makroskopisches, modulares Betonmodell für Hydrocodes mit Verfestigung, Scädigung, Entfestigung, Drei-Ivariantenabhägigkeit und Kappe, Berich 7/98, Fraunhofer Institut für Kurzzeitdynamik-Ernst-Mach-Institut, Freiburg i. Br 1998.
[26] Camacho GT, Ortiz M. Adaptive Lagrangian modelling of ballistic penetration of metallic targets. Comput Methods Appl Mech Eng 1997;142:269–301.
[27] Børvik T, Langseth M, Hopperstad OS, Malo KA. Ballistic penetration of steel plates. Int J Impact Eng 1999;18(2): 855–86.
[28] Bischoff PH, Perry SH. Compressive behaviour of concrete at high strain rates. Mater Struct, RILEM 1991;24:425–50.
[29] CEB. Concrete structures under impact and impulsive loading. CEB bulletin d'information No. 187, Laussanne, Switzerland, 1988.
[30] Hillerborg A, Modeer M, Petersson PE. Analysis of crack formation and crack growth in concrete by means of fracture mechanics and finite elements. Cement Concr Res 1976;6:773–82.
[31] Rots JG. Computational modeling of concrete fracture. PhD dissertation, Delft University of Technology, Department of Civil Engineering, Delft, The Netherlands, 1988.
[32] FIB/CEB State of the art report: high strength concrete, Switzerland, 1990.
[33] Sellevold E, Justnes H, Smeplass S, Hansen EA. Selected properties of high performance concrete. In: Grutzek MW, Sarkar SL, editors. Advances in cement and concrete. New England: ASCE; 1994. p. 562–609.
[34] Hanchak SJ, Forrestal MJ, Young ER, Ehrgott JQ. Perforation of concrete slabs with 48 MPa and 140 MPa unconfined compressive strengths. Int J Impact Eng 1992;12(1):1–7.